Structural and dynamic studies of water in mesoporous silicas using neutron scattering and nuclear magnetic resonance

2004 J. Phys.: Condens. Matter 16 S5449

(http://iopscience.iop.org/0953-8984/16/45/009)

INSTITUTE OF PHYSICS PUBLISHING JOURNAL OF PHYSICS: CONDENSED MATTER

J. Phys.: Condens. Matter **16** (2004) S5449–S5470 PII: S0953-8984(04)78970-5

Structural and dynamic studies of water in mesoporous silicas using neutron scattering and nuclear magnetic resonance

Beau Webber and John Dore

School of Physical Sciences, University of Kent, Canterbury, Kent CT2 7NR, UK

E-mail: J.C.Dore@kent.ac.uk

Received 5 April 2004, in final form 15 September 2004
Published 29 October 2004
Online at stacks.iop.org/JPhysCM/16/S5449
doi:10.1088/0953-8984/16/45/009

Abstract

Experimental techniques for studying the behaviour of water in confined geometry using neutron scattering and NMR methods are reviewed. A brief survey is given of earlier work on sol–gel silicas and these findings are updated by reference to current work on MCM- and SBA-type silicas. Particular attention is focused on the phase transitions and the relation between supercooled water and ice phases in the confined geometry of the mesopores. The characteristics are found to behave in a systematic manner although the nucleation phenomenon for partially filled pores reveals some unexpected complexity for the SBA silicas.

(Some figures in this article are in colour only in the electronic version)

1. Introduction

An interest in the behaviour of liquids, especially water in confined geometry, has grown rapidly over the last decade, covered in general review (Christenson 2001). This research has progressed due to the development of well characterized micro- and mesoporous solids with a defined pore structure, coupled to an increased range of possible applications due to the modified properties of the confined phase.

Experimental techniques for studying the properties have similarly undergone a significant advance during this period. The use of neutron diffraction to investigate the structural features of water in various mesoporous silicas has been reviewed in an earlier paper (Dore 2000) and more recent work is provided in the following sections to update this work. One of the newer techniques has been the development of NMR methods (McDonald and Strange 1998) and the advances made in this area are also included. The complementarity of different methods is seen as an important aspect in the development of a greater understanding of the factors involved in the modified characteristics.

2. Experimental techniques and theoretical background

2.1. Neutron diffraction and small-angle scattering

Neutron diffraction has been used extensively for the structural investigation of molecular materials (Dore 1991) and only a brief survey of the formalism will be given here. The measured intensity pattern for a liquid is converted to a structure factor, $S_{\mathrm{M}}(Q)$, that contains intra- and inter-molecular terms:

$$S_{\mathrm{M}}(Q) = f_1(Q) + D_{\mathrm{M}}(Q). \tag{1}$$

The inter-molecular function, which defines the structure, can be transformed to give the orientationally averaged spatial correlations by the Fourier relation

$$d_{\mathrm{L}}(r) = 4\pi r\rho_0[\overline{g(r)} - 1] = \frac{2}{\pi}\int_0^\infty Q D_{\mathrm{M}}(Q)\sin Qr\,\mathrm{d}Q. \tag{2}$$

In the case of confined liquids, a similar analysis procedure is carried out but it is necessary to subtract the scattering pattern for the dry substrate from the measurements. The scattering from the silica plus water contains cross-terms from the spatial correlations between the water/ice and the silica. Subtraction of the dry silica scattering to give the pattern for the adsorbed phase does not remove these terms. In the case of large pore sizes with fully filled pores the contribution is negligible, but for small pores the contribution may be significant, particularly if there are strong correlations across the interface. Although both the water and the silica are disordered materials, hydrogen-bonding, arising from surface hydroxyl groups, will produce local correlations that will contribute to the measured interference function. The size of this contribution depends on a number of different factors and may result in significant effects that can impact on the interpretation of the results.

The first effect on the diffraction pattern for the confined water is due to the dispersed nature of the water/ice volume. The scattered distribution for the water/ice is not equivalent to that for a homogeneous bulk sample even if the structural features are unchanged. The observed intensity will exhibit diffraction broadening arising from a convolution of the full pattern with a function that represents the mesoscopic distribution of the water in the pores. This broadening effect, which is equivalent to the Debye–Scherrer effect for crystalline materials, is inversely proportional to the size of the pores (and relates to the small-angle scattering profile of the silica matrix). Fully filled pores of <50 Å size are unlikely to produce any measurable effects in the pattern for water on a typical medium-resolution instrument. The situation for the ice is different as the Bragg peaks are much sharper and the broadening effects become more apparent. However, the ice phase is itself disordered and the detailed treatment of the intensity profile for this case, as measured on a high-resolution instrument, has not yet been fully addressed. Consequently, it is normally assumed that the diffraction broadening effects do not cause a significant change in the pattern unless the pore size is below $\sim$30 Å; more detailed information from partially filled samples involving larger pore sizes may subsequently cause a re-evaluation of this position.

From the experimental point of view, there is no alternative to the 'wet–dry' analysis technique so the separation of the interfacial layer contribution to the observed intensity cannot be directly determined without making some assumptions or approximations. Several papers have addressed this issue (Steytler *et al* 1983, Bruni *et al* 1998, Soper *et al* 1998), and more recently (Morineau and Alba-Simionesco 2003), but there is no established analytic method that can be universally applied to the various datasets. Furthermore, the interfacial correlations are expected to be strongly dependent on various parameters, such as the surface hydroxyl density and the strength of the wetting interaction, so the corrections are sometimes directly linked to

the features being investigated. Fortunately, the cross-correlation contributions can often be neglected as they are small for studies involving larger pore sizes but their possible presence needs to be taken into account in the interpretation of the results. These features are discussed for specific samples in section 3.1.

The use of a temperature difference technique alleviates some of the problems arising from the evaluation of the absolute structure factor for the confined water/ice. In this case, the substrate scattering is completely eliminated and also the cross-correlation contributions to the first-order. If, as is commonly assumed, there is an interfacial water layer at the interface that is not greatly affected by temperature changes, then this contribution is also conveniently removed along with the silica scattering by taking differences in the scattering intensity at different temperatures. Furthermore, if it is assumed that after nucleation the main volume of the ice in the centre of the pore is not undergoing any structural change other than expansion/contraction, the temperature difference function in the low temperature region becomes highly sensitive to possible changes in the interfacial layer. These issues are discussed more fully in section 4 for the various samples considered in this paper.

For neutron scattering it is usual to use D_2O water to avoid the complications of incoherent scattering and inelasticity corrections that arise in the case of H_2O. This procedure is in contrast to the NMR measurements where the higher magnetic moment of the protons in H_2O water makes this the preferred choice. For D_2O, the composite pair correlation function extracted from the neutron data is

$$\overline{g(r)} = 0.111 g_{\mathrm{OO}}(r) + 0.445 g_{\mathrm{OD}}(r) + 0.444 g_{\mathrm{DD}}(r) \tag{3}$$

so that the measurement is sensitive to the orientational correlations between neighbouring hydrogen-bonded molecules. Liquid water shows substantial local ordering (Dore 1985, Soper 1994, Dore and Blakey 1995) under ambient conditions and this feature is enhanced as the temperature is reduced (Sufi 1984, Dore *et al* 2000).

A convenient way of investigating structural change is through the temperature-difference function (Gibson and Dore 1983), defined in relation to a reference temperature, T_0, by

$$\Delta D_{\mathrm{M}}(Q, T; T_0) = S_{\mathrm{M}}(Q, T) - S_{\mathrm{M}}(Q, T_0); \tag{4}$$

this function is less susceptible to systematic errors than $S_{\mathrm{M}}(Q)$.

These expressions also apply to the crystalline ice phase but it is more usual to analyse the diffraction pattern in terms of Bragg peaks corresponding to the lattice structure. Crystalline hexagonal ice, I_h, has a well defined set of peaks with a characteristic triplet centred on a Q-value of 1.7 $\mathrm{Å}^{-1}$. Cubic ice, I_c, has only a single central peak in this Q-value region, and is metastable with respect to ice I_h. Both forms of ice are created in the present experiments and the cubic ice always shows a defective form, which will be discussed in later sections. The positions of the peaks define the lattice constants and their variation with temperature shows how the lattice contracts with reducing temperature.

The intensity profile of the Bragg peaks also gives information about the crystalline phase through the Debye–Scherrer equation that relates the width of the peak, $\sigma(Q)$, to the number of correlated planes and, consequently, the inverse of the crystallite size, D, such that

$$\sigma(Q) = \frac{4\pi K_{\mathrm{DS}}}{D}, \tag{5}$$

where K_{DS} is a constant dependent on the shape of the crystallite. For a spherical-shaped crystallite $K_{\mathrm{DS}} \approx 1$, but for the long cylindrical structures expected in SBA-15 pores, K_{DS} will be an orientational average over various dimensions and could also depend on preferred directional growth within the pores. However, it seems unlikely that K_{DS} will vary much from unity for the powdered samples considered here.

The temperature-difference function is particularly useful in studies of phase transformations in confined geometry since the amount of material in the beam is not influenced by density changes. The liquid phase has a broad oscillatory structure that is easily distinguished from the relatively sharp peaks of the crystalline phase. Under these conditions the growth of the peaks under cooling conditions gives a direct quantitative indication of the formation of the solid phase, including any defects in its structure. In a similar fashion, the melting of the solid phase is revealed in the warming sequence, and shows any hysteresis effects in the transformations.

Small-angle neutron scattering (SANS) has been used primarily to characterize the pore structure of the materials. At low Q-values, typically <0.2 Å^{-1}, the intensity profile may be written in general terms (Dore and North 1991) as

$$I(Q) = \int_V \rho(\mathbf{r}) \exp(\mathrm{i}\mathbf{Q} \cdot \mathbf{r})\, \mathrm{d}^3\mathbf{r} \tag{6}$$

where $\rho(\mathbf{r})$ is the spatial distribution of coherent scattering from different regions of the sample. For a two-component system represented as a solid matrix and a void region of isolated spherical pores, this integral expression is separable in the moderately dilute limit and may be approximated by

$$I(Q) \sim (\Delta\rho)^2 \, |F(Q, R)|^2 \, P(R) S_c(Q) \tag{7}$$

where $\Delta\rho$ is the contrast or difference in the mean coherent scattering amplitudes for the two components, $|F(Q, R)|$ is a form factor characterizing the shape of the pores, $P(R)$ represents the distribution of pore sizes, and $S_c(Q)$ represents the spatial distribution of the pore centres. It is necessary to choose a suitable expression for $P(R)$ in order to extract the desired structural parameters from the observations.

For real porous systems, the expression in equation (7) may not satisfy the dilute limit and other approaches may be necessary. Monte Carlo techniques and direct integration may be used to model disordered pore networks and the SANS intensity profile can be evaluated from the Fourier transform of the associated spatial correlation function $\gamma(r)$. Combined with density and NMR cryoporometry information, Monte Carlo integration calculations have been used to interpret the neutron scattering for several dry sol–gel silica samples, covering both the SANS and diffraction regimes ($Q = 8 \times 10^{-4} \rightarrow 17$ Å^{-1}), (Webber 2000, Webber *et al* 2001). This study also treated the case of uniaxial cylinders on an hexagonal lattice, characteristic of the ordered MCM-41 (and SBA-15) mesoporous silicas. As expected the model parameters required much lower variances for pore diameter and spacing when fitting the scattering from the latter silica types than in the case of sol–gel silicas.

For liquids in pores, an analytic formalism has been developed (Bruni *et al* 1998, Soper *et al* 1998, Morineau and Alba-Simionesco 2003), using a structure factor corresponding to the lattice arrangement, convoluted with a form factor for the pore diameter. The effects of 'excluded volume' and liquid–substrate 'cross-correlations' are discussed in relation to specific studies of water in Vycor glass (Bruni *et al* 1998) and benzene in MCM-41 and SBA-15 silicas (Morineau and Alba-Simionesco 2003). It is suggested that changes to the bulk diffraction pattern due to the confinement for these samples may be comparable to the changes from possible structural modification. This approach may be useful for the detailed analysis of the supercooled water results, particularly under conditions of partial filling, but is unlikely to influence the conclusions about the phase transformations.

The contrast value, $\Delta\rho$, can be varied by filling the pore volume with a liquid, and the use of H/D isotopic substitution enables the contrast-matched method ($\Delta\rho = 0$) to be achieved for most porous materials (excluding the activated carbons) (Dore *et al* 1995, Farman *et al* 2002). This technique can also be used to investigate the partial filling of the pores but little

experimental work has so far been reported for this three-component (solid matrix, fluid, void) system.

2.2. NMR relaxation, diffusion and cryoporometry studies

There has been a wide range of nuclear magnetic resonance investigations into the properties of water/ice systems in confined geometry, using the following five main techniques.

- Measurement of changes in the lineshape (in the frequency domain) due to the magnetic susceptibility field gradients that are present in porous systems (Bahceli *et al* 1991, Allen *et al* 2001). In high NMR static magnetic fields, diffusion in these gradients may dominate the NMR relaxation of liquids in pores.
- Measurement of changes in the T_1 (longitudinal or spin–lattice) and T_2 (transverse or spin–spin) relaxation times (in the time domain) due to exchange of magnetization between the liquid in the pore and the pore wall (Brownstein and Tarr 1977, Halperin *et al* 1991, Strange *et al* 1996b, Stapf *et al* 1996, Allen *et al* 1998, Booth and Strange 1998a, 1998b, Allen *et al* 2001, Levitz *et al* 2003, Strange *et al* 2003, Alnaimi *et al* 2004). In low NMR static magnetic fields, this exchange of magnetization tends to dominate the NMR relaxation of liquids in pores.
- Variation of the amplitude of the liquid component in the T_2 relaxation curve with temperature, and the interpretation of this in terms of the Gibbs–Thomson relationship—NMR cryoporometry (Strange *et al* 1993, Overloop and van Gerven 1993, Alnaimi *et al* 1994, Hansen *et al* 1996, Allen *et al* 1998, Webber 2000, Webber *et al* 2001, Strange *et al* 2003, Alnaimi *et al* 2004).
- Measurement of translational diffusion of the confined water using pulsed magnetic field gradient or fringe magnetic field gradient techniques (Mitzithras *et al* 1992, Codd and Callaghan 1999, Stallmach and Kärger 1999, Paoli *et al* 2002, Kimmich 2002, Callaghan *et al* 2003, Valiullin *et al* 2003, Geier *et al* 2004).
- Direct measurement of the nuclear magnetization transfer as a function of time (Gore *et al* 2001, Valiullin *et al* 2003).

Most of these techniques are to some degree equivalent in that they determine the dynamical processes by measuring the transfer of nuclear spin magnetization and thus the coupling between different parts of the system being studied. In the present case the magnetization transfer is essentially between the water, the ice and the containing silica surfaces, as mediated by diffusion and modified by re-orientational averaging. As a result, these techniques are highly sensitive to the state of the water/ice at the silica surfaces, which may be in a significantly different thermodynamic state to bulk water/ice. The diffusion measurements in particular point to the existence of a mobile component for the water/ice system in pores.

The prime features dominating the measured NMR relaxation are well understood but further developments will be needed to relate the details in individual confined geometry systems to the basic physical processes. The direct measurement of the magnetization transfer is proving highly informative for the study of liquid–substrate interactions in porous media. A technique that is proving invaluable is thermoporosimetry/NMR cryoporometry. J W Gibbs, J Thomson, W Thomson (later Lord Kelvin) and J J Thomson employed thermodynamics, generalized dynamics and experimentation to develop an understanding of the effects that a range of variables, including geometry, have on basic properties of matter such as vapour pressure and melting point (Gibbs 1906 reprinted 1961, 1928, Thomson 1849, 1862, 1871, 1888). In particular, they established that the melting point depression for a small crystal varies inversely with crystal diameter. This behaviour is closely related to the capillary effect and

both reflect the change in bulk free energy caused by the curvature of an interfacial surface under tension (Defay *et al* 1951, 1966, Gregg and Sing 1967). Consequently, the Gibbs–Thomson equation for the melting point depression, ΔT_m, for a small crystal of diameter x may be written (Jackson and McKenna 1990) as

$$\Delta T_m = T_m - T_m(x) = \frac{4\sigma_{cl} T_m}{x \Delta H_f \rho_s} \tag{8}$$

where T_m is the normal melting point of bulk liquid; $T_m(x)$ is the melting point of crystals of diameter x; σ_{cl} is the surface energy at the crystalline–liquid interface; ΔH_f is the bulk enthalpy of fusion (per gram of material); ρ_s is the density of the solid.

This expression may be written more simply as

$$\Delta T_m = \frac{k_{GT}}{x} \tag{9}$$

where k_{GT} is a calibration constant to be determined. The Gibbs–Thomson equation is the constant pressure variant of a set of thermodynamic equations (Gibbs 1906 reprinted 1961, 1928), whereas the Kelvin equation (Thomson 1871, equation (2), p 450), (Thomson 1888, equation (171), p 163) is the constant temperature variant.

The above equations show k_{GT} is dependent only on the properties of the liquid and its interfacial interaction with its own solid. The Kelvin equation applies to an isolated droplet in its own vapour, and thus to a right cylindrical void containing a hemispherical interface between a completely wetting liquid and its own vapour (Thomson 1888, pp 163, 164); similarly, the Gibbs–Thomson equation applies to a spherical crystal in its own liquid, and thus to a right cylindrical void containing a hemispherical interface between a non-wetting crystal and its own liquid. It should be noted that the above model for the Kelvin equation applies to the evaporation branch of the absorption isotherms (Coelingh 1938, Cohan 1938), (Gregg and Sing 1967, p 146).

In general, in a porous solid, there is also a contribution from crystalline–substrate and liquid–substrate interaction terms. These terms may, with good approximation, be represented as an additional $\cos\phi$ term in the Gibbs–Thomson equation and the related Kelvin equation, where ϕ is the wetting or contact angle, commonly assumed to be 0° in the Kelvin case and 180° in the Gibbs–Thomson case (Young 1805), (Young 1855, VII—Cohesive Attraction of Solids and Fluids pp 432–6, partially ascribed to Clairaut), (Gregg and Sing 1967, equations (3.1), (3.2), (3.27), pp 123, 135–136, 150–156), (Tell and Maris 1983, equation (2)), (Jackson and McKenna 1990, p 9002), (Martin *et al* 2002). This $\cos\phi$ term also has a straightforward geometric interpretation since a spherical meniscus of radius r_1, in a cylindrical capillary of radius r, with an angle of contact ϕ, has $r = r_1 \cos\phi$ (Gregg and Sing 1967, figure 3.14, p 143).

As indicated above, the Kelvin and Gibbs–Thomson equations apply to right cylindrical pores. In the general case, the influence of pore geometry must also be taken into consideration, resulting in a change of value of the numerical constant '4' in equation (8). Hence, x is used in the above equations as opposed the more specific radius R or diameter D, that is used elsewhere. It is also clear that deviations from the thermodynamic ideal can be expected for small dimensions where the molecular features of the confined phase are comparable with the pore size (Gelb *et al* 1999, Sliwinska-Bartkowiak *et al* 1999, Webber 2000, Webber *et al* 2001). These points are discussed further in sections 4.3 and 5.

Studies of the change in the melting temperature of liquids for confined geometry were originally performed using differential scanning calorimetry (DSC), and termed thermoporosimetry (Brun *et al* 1977, Eyraus *et al* 1988, Jallut *et al* 1992). However, other techniques for determining the melting features can be used, and NMR relaxation

measurements offer a convenient alternative. The technique of NMR cryoporometry (Strange *et al* 1993, Alnaimi *et al* 1994, Strange 1994) directly measures the quantity of the liquid that is present inside the pore matrix and can readily provide a quantitative measure of the pore volume per gram of porous solid. The reorientational motion in a liquid results in a longer NMR T_2 relaxation time than in the solid. NMR cryoporometry makes use of this change to determine the quantity of the liquid phase as a function of temperature. At short times the signal from both the crystalline and liquid phases are present and at much longer times the signal from both will have decayed. By measuring the amplitude of the signal in an appropriate intermediate range of times, as a function of temperature, NMR cryoporometry determines the fraction of the total liquid that has melted at a particular temperature. Applying the Gibbs–Thomson transformation enables the pore size distribution to be evaluated.

This method has some advantages over the DSC thermoporosimetry studies as DSC involves a dynamic (differential) measurement that depends on energy transfer, whereas the NMR cryoporometric signal is a static amplitude that may be measured directly. In NMR studies, the warming rate can be varied arbitrarily to reveal the sharpest transitions for a wide range of pore distribution functions or to signal-average over longer times to measure small pore volumes. The DSC method is constrained by the dynamic nature of the signal and thus it cannot always measure adequately slowly to fully resolve sharp transitions. DSC may also fail to reveal the broad transitions characteristic of deep melting point depressions, due to the low heat flux.

NMR cryoporometry also has a unique advantage in that it can be combined with standard NMR imaging techniques to determine the spatial distribution of the pore sizes throughout the volume of the sample (Strange *et al* 1996a, Strange and Webber 1997a, 1997b).

3. Previous results

It is convenient to use D_2O for the neutron measurements as hydrogen has a large incoherent scattering cross-section that contributes a large background to the observed intensity pattern. H_2O is preferred for the NMR measurements because the higher magnetic moment gives rise to a higher signal-to-noise ratio, although deuterium NMR is being increasingly used to study water in confined geometry (Hansen *et al* 2002).

There is a significant debate about possible differences in the structural features of light and heavy water but most thermo-physical properties seem to be equivalent with a temperature difference in the region of 5 °C. The melting point of bulk D_2O is 3.82 °C compared with 0 °C for H_2O and the point of maximum density is 11 °C for D_2O compared to 4 °C for H_2O. For the purpose of the present studies, where the effects of temperature variation are investigated, it is satisfactory to assume that the changes relating to the ΔT variable (with different T_0 chosen on the basis of the bulk melting point) are equivalent even though there will be differences on an absolute temperature scale.

3.1. Sol–gel silicas

Much of the earlier neutron scattering and NMR work centred on the sol–gel silicas, which have a wide range of pore sizes. The findings have been published in a number of papers and reviews (Dore 2000, Webber *et al* 2001, Allen *et al* 2001, Alnaimi *et al* 2004).

The neutron results may be summarized as follows:

- the nucleation point, corresponding to the formation of ice, is depressed by an amount ΔT that depends on the pore size, geometry and fractional filling,

- the main diffraction peak of water in the confined state, $Q_0(T)$, is displaced to lower Q-values with respect to that for bulk water and then further as the temperature is reduced,
- the 'supercooled' water shows enhanced hydrogen-bonding as the temperature is reduced,
- nucleation leads to the formation of a defective form of cubic ice for pore diameters of $D < 300$ Å; for larger pores, even a thin film of liquid at the interface produces the normal form of hexagonal ice,
- cooling and warming cycles show that there is hysteresis in the nucleation and melting of the ice (but not for MCM silicas).

There has been considerable research into the structure and the dynamics of water/ice systems in sol–gel systems, using a range of NMR techniques. The overall features from the NMR studies may be summarized as the following.

- The depression of melting point, ΔT, follows the Gibbs–Thomson relationship and is inversely proportional to the pore diameter, D.
- The freezing point (cooling run) is depressed by an amount due to both the Gibbs–Thomson effect and to an additional effect arising from the supercooling of the liquid state; more consistent measurements are therefore obtained from the melting process during a warming run.
- Diffusional processes within the pore magnetic susceptibility gradients result in a magnetization decay that is initially quadratic, but at larger time decays $\propto \exp(-t/\tau)^3$. This effect may dominate in high magnetic field NMR. (In closed pore systems the diffusion is bounded and the decay rate is then in this longer limit determined by the other processes discussed here.)
- The T_2 relaxation time of the water in the pores is reduced due to magnetization exchange between the protons and surfaces. This effect may dominate in low magnetic field NMR.
- The T_2 relaxation time of the ice formed in the pores is increased over the value for bulk ice due to an increased proton mobility; this behaviour may be due to both an ice–surface interfacial layer with an increased mobility and/or an increased mobility in the body of the pore ice due to defects.
- Water/ice systems in pores show an increased diffusion rate compared with bulk ice, usually assumed to be due to a mobile surface layer.

It has been confirmed experimentally (Hansen *et al* 1996, Webber 2000, Webber *et al* 2001) that the melting point of water in a range of porous materials varies closely with the inverse of the pore diameter, although there are indications that pores of differing geometry and surface properties may require different k_{GT} values, as expected.

Figure 1 shows a comparison of the ΔT values for NMR measurements of the melting point depression of water in confined geometry, against the inverse pore diameter as determined by gas adsorption measurements, for a range of sol–gel silicas with characteristic pore sizes of 25–500 Å, measured at $2\tau = 4$ ms. (Webber 2000, Webber *et al* 2001). These results were found to be independent of the measuring time for $2\tau = 4 \rightarrow 40$ ms, and show good agreement with the Gibbs–Thomson relationship. The results suggest that a value for k_{GT} of 582 K Å is appropriate for water in sol–gel silicas. Both preliminary measurements in this work (1994), and measurements by others in smaller pores employing different 2τ times probing other dynamical process rates (Hansen *et al* 1996), have suggested that k_{GT}/x in the Gibbs–Thomson expression may be replaced by $k_{GT}/(x - x_{sl})$, where it has been assumed that x_{sl} is related to a non-frozen layer. However, there is a need to evaluate the full amplitude versus time relaxation curve for these water/ice systems in confined geometry, to correctly interpret the NMR information. The NMR relaxation measurements for SBA silica, discussed in sections 4.3, 4.4, throw further light on this point.

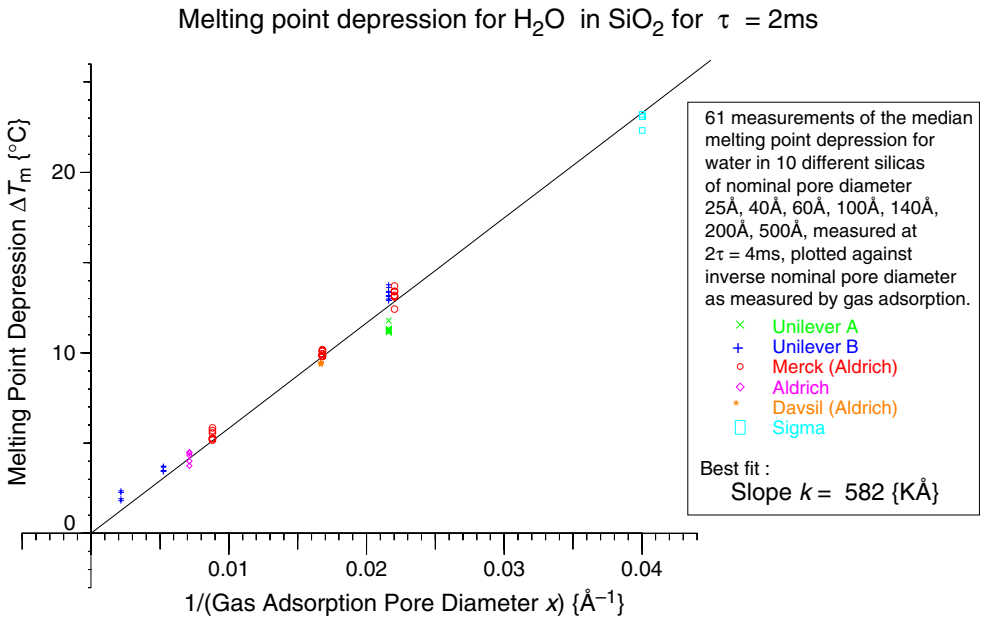

Figure 1. The relation of melting point depression to inverse pore diameter for water in various sol–gel silicas of diameter 25–500 Å, as calibrated by gas adsorption.

The NMR cryoporometry results indicate that a typical sol–gel silica has an approximately Gaussian (normal) pore diameter distribution, with $\sigma/D \sim 0.1 \rightarrow 0.2$ i.e. a full-width at half-height typically of the order of one third of the pore diameter (Webber 2000). Hence measurements parametrized as a function of pore diameter are inevitably convoluted with this broad pore distribution. These effects are particularly important in the investigation of the interactions between the water/ice system and the silica surface, since measurements made as a function of pore filling factor, f, imply different quantities of water in different sized pores. Consequently, it is not easy to separate the change in the properties for a given temperature and pore diameter from that caused by the range in pore diameters for a given sol–gel sample.

While the work on sol–gels characterizes these individual systems well, there is an interpretation problem for the small pores arising from the wide distribution of pore sizes in an individual sol–gel sample. These effects are particularly important in the investigation of the interactions between the ice/water system and the silica surface, as a function of pore diameter. A detailed interpretation of the behaviour will probably require a co-ordinated investigation using different experimental probes for both the structural and dynamic characteristics. The complementarity of the neutron and NMR techniques has already been discussed in earlier papers (Webber *et al* 2001, Strange *et al* 2003, Dore *et al* 2004).

An interesting recent study of water in sol–gel silicas has been reported by the Messina group (Crupi *et al* 2003) using both neutron diffraction and quasi-elastic/inelastic neutron scattering. The silica sample was a porous glass, GelSil, which has a nominal pore diameter of 26 Å with a fractal network and was studied for filling factors of $f = 1.00, 0.95, 0.05$, over the temperature range -30 to 40 °C. In this case, a large proportion of the water volume is close to the interface and an attempt to evaluate the water–silica cross-correlations was made using the data obtained from the $f = 0.05$ measurements. Systematic variations in $d_l(r)$ are observed with temperature but the results are not interpreted in terms of the difference technique so the

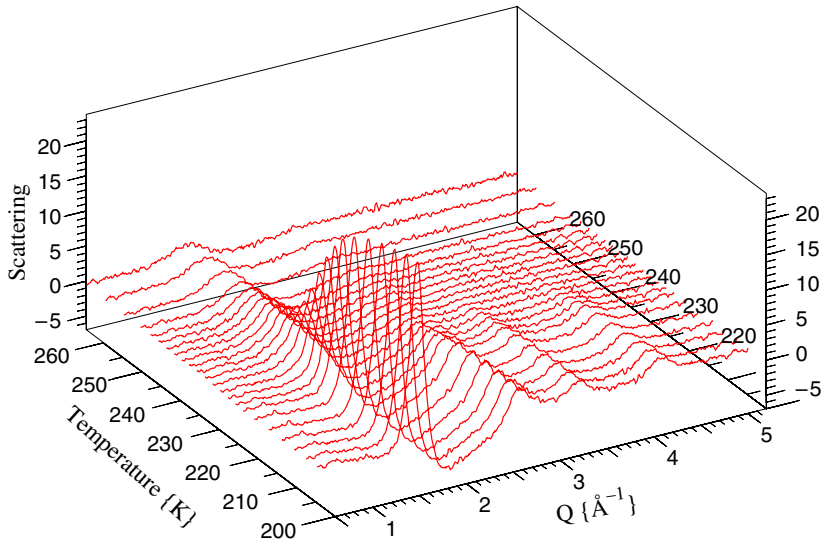

Figure 2. The variation in the neutron diffraction pattern from D_2O water/ice in an MCM silica as a function of temperature.

detailed changes within the hydrogen-bonded network are not extracted. The amount of cubic ice formed at the lowest temperature is quite small, suggesting that full nucleation has not occurred or that the crystallite size is much smaller than the pore size. The results are broadly in agreement with the earlier diffraction studies of sol–gel silicas (Dore 2000) and extend the range of investigations to low pore sizes.

The IQENS and IINS measurements for these samples allow an investigation of the dynamic properties and have been interpreted in terms of hindered rotation and changed vibrational features for the confined state. The results are shown to be closely related to the extensive studies of the Messina group using Rayleigh wing scattering (Crupi *et al* 2003) and there are now several different experimental probes of the dynamical features. The overall conclusions seem to be that the diffusion for water is hindered by the confinement and the specific effects of surface interactions and also that the relaxation processes show a wide range of timescales that can be treated in the context of mode coupling theory. NMR magnetic field gradient techniques listed earlier also show a hindered diffusion in water, but in frozen systems show an increased diffusion above that expected for ice, usually assigned to a more mobile surface layer. This feature is discussed further in sections 4.3 and 4.4.

3.2. MCM and SBA silicas

The production of ordered mesoporous silicas such as MCM41 and MCM48 by a templating process led to an extended study involving cylindrical pores with pore diameters in the region of 25 → 35 Å. In this case the ice nucleation is considerably depressed and the liquid state can exist in the pores at a temperature of 45 °C below the bulk freezing point! The neutron results (Dore *et al* 1999, Dore 2000, Dore *et al* 2004) showed that there is no hysteresis in these cases when the pores are filled. An initial report of temperature variation studies that compare the results for MCM and sol–gel silicas has been published (Dore *et al* 2002b). The results for an MCM silica with a pore diameter of 35 Å are shown as a temperature difference plot in figure 2.

More recently, the fabrication of a relatively new type of ordered mesoporous silica through polymer templating, known as SBA-15 silica, has extended the pore range up to nearly 100 Å. This development has opened up new possibilities, which are discussed in the subsequent sections. Findenegg and colleagues (Schreiber *et al* 2001) have made a systematic study of water in both MCM and SBA silicas using a range of different experimental techniques. The results obtained for the DSC and SANS measurements indicated a varying behaviour with respect to silica type, pore radius and water filling factor. The details of this investigation are described in subsequent sections. A recent x-ray study of water/ice in SBA-15 silica (Morishige and Iwasaki 2003), involving a range of different filling factors, is discussed in section 4.2.

3.3. Phase relations for confined water/ice

The process of ice formation in confined geometry has been investigated in earlier temperature-variation studies (Baker *et al* 1997, Dore *et al* 2002a, 2002b) and it was found that a defective form of cubic ice is always created in pores with a mean diameter D of less than 300 Å. It has been suggested that the proto-crystal formed in the liquid state is effectively a disordered hydrogen-bonded cluster of water molecules that does not possess well defined crystallographic axes. The regular stacking of the *ababab* sequence of hexagonal ice is therefore not created in this initial phase. As the hydrogen-bonded cluster grows into a small crystallite, there is preferential growth in certain directions, which establishes the direction of the crystallographic axes but does not differentiate between them due to the stacking faults. It is only when the crystallite has reached a critical size that the variable growth rates in different crystal planes can be effective. It therefore seems likely that all ice crystals start their life as a defective cubic ice crystallite and this behaviour is revealed in the confined geometry only because the eventual size of the crystal is restricted to the limits imposed by the pore dimensions.

In this context, the geometrical nature of the pore network and the water filling factor may be important as they will define the way that the interface between the water and the ice can change. The sol–gel silicas have a range of pore sizes connected by narrow openings or channels but it seems that there is no connectivity in terms of the nucleation event and the crystallites in neighbouring pores are independently formed. The situation in ordered cylindrical pores is distinctive as, although the pore size is small in two directions, there is an extensive pore volume without any constrictions extending along the cylinder axis. In these circumstances it is feasible that there will be a different behaviour in the growth process and the characteristics will also be dependent on the filling factor f.

4. New results for SBA silicas

4.1. Sample preparation

Two SBA-15 samples were provided by Findenegg and colleagues (Schreiber *et al* 2001, Findenegg, private communication) and characterized by gas adsorption, DSC and SAXS using a Kratky camera: BJH N_2 condensation data indicates for sample A a pore diameter D_p of 91 Å, $A_s = 902 \pm 50$ m^2 g^{-1}, $V_p = 1.31 \pm 0.07$ ml g^{-1}, and for sample B a pore diameter D_p of 62 Å.

4.2. Neutron studies

Neutron diffraction measurements have been made for these two samples of SBA-15 silica. The data were measured on the D20 diffractometer (Hansen 2004) at the Institut Laue Langevin,

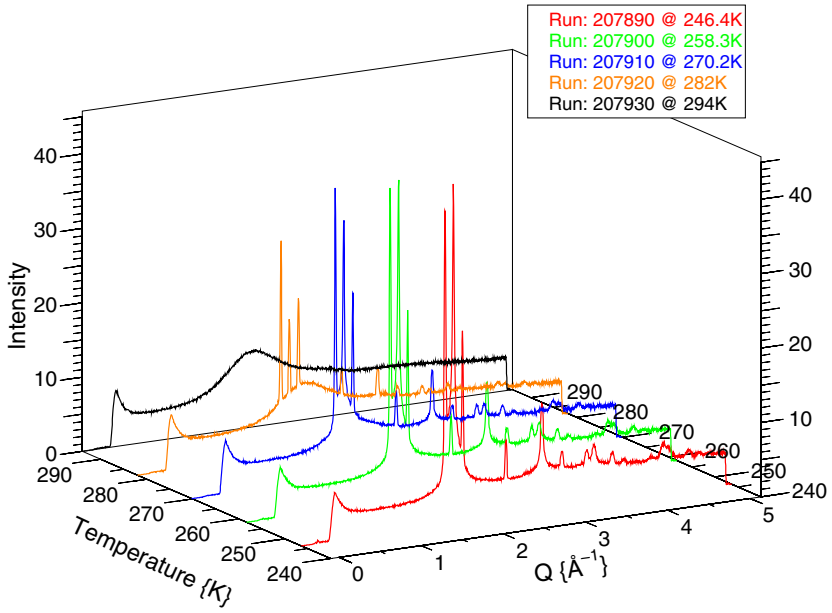

Figure 3. The diffraction pattern for water/ice in an overfilled sample of SBA-15 silica (sample A1) as a function of temperature during a warming ramp.

Grenoble, using an incident wavelength of 2.4 Å. The use of a longer wavelength than in the earlier studies provided an improved Q-resolution in the intensity profile of the Bragg peaks and consequently gives additional information on the effects of disorder in the cubic ice pattern and the diffraction broadening due to crystallite size restrictions. In addition to the neutron scattering data, some of which will be reported later, and gas adsorption and DSC measurements (Findenegg, private communication), some complementary NMR measurements were also made after the main neutron experiment. These measurements are discussed in section 4.3.

Several pore fillings were used for each of the samples but results are presented here for only two of the cases studied, both for SBA-15 with a pore diameter of 91 Å:

(A1) with $f = 1.13$, corresponding to an overfilled case, and
(A2) with $f = 0.61$, corresponding to a partially filled case.

Measurements were usually made for a temperature ramp of ± 0.6 K min^{-1} in either cooling or warming mode and corrections were made for the thermal lag in the sample.

Figure 3 shows the measured diffraction pattern for sample A1 at various temperatures during a warming cycle. The figure shows the presence of several different phases corresponding to liquid (D_2O) water, hexagonal ice and cubic ice at various temperatures. There is a broad peak for the water pattern in the liquid phase (294 K) and at lower temperatures there are ice peaks. At 282 K, the characteristic triplet of hexagonal ice is clearly visible at 1.64, 1.75, 1.86 Å^{-1}, with additional single peaks at 1.99, 2.82, 3.06, 3.36, 3.46, 3.67 Å^{-1}, superimposed on a significant water peak. At lower temperatures there is a broader peak structure characteristic of defective cubic ice, showing additional peaks under the triplet and at 2.83, 3.46 Å^{-1}. A more detailed discussion of the control system and measurement sequence will be presented separately.

The results show unambiguously that the hexagonal ice has no melting point depression and is thus forming in the excess water around the grains of silica, whilst the melting of the

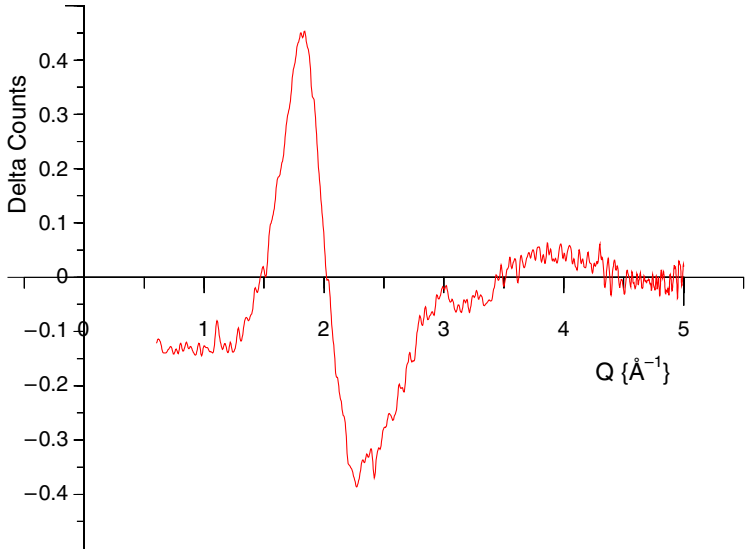

Figure 4. The temperature difference function for the liquid phase in SBA-15 (sample A1), for $\Delta T = 24$ K, $T_0 = 296$ K.

defective cubic ice shows a Gibbs–Thomson depression ΔT_{GT} of 14.0 °C, in close agreement with that seen by NMR, and is thus forming in the pores.

The changes occurring in the liquid region are shown in figure 4, where $\Delta D_M(Q, T; T_0)$ is plotted for a ΔT value of 24 K and reference temperature T_0 of 296 K. The variation in peak position $Q_0(T)$ gives the characteristic differential form and the shape is similar to that obtained in previous work (Dore 2000). It is notable that the scattering in the low-Q region has a variable level. This effect is reproduced in figure 4 as a finite displacement that is seen for all studies of supercooled water and has been attributed to a reduced isothermal compressibility as the temperature is reduced. However, this region of the Q-scale does not strictly correspond to the limiting situation of $Q \mapsto 0$, so this behaviour is an indication of the trend in the long-range features of the liquid phase, which eventually reduces further as the ice forms in the pores. It therefore seems that the structural changes in the liquid phase are consistent across the bulk and confined systems, but displaced in an absolute temperature scale.

The changes in the diffraction pattern as a function of the temperature for the region of the main peaks are displayed in figure 5. The sequence illustrates the difference between the liquid phase, the composite phase where the hexagonal ice has formed outside the pores but there is still a liquid phase in the pores and the phase showing the characteristic triplet shape of a defective form of cubic ice at 1.6–1.9 Å^{-1}. The hexagonal ice peaks are sharp, indicating a large crystallite size, and the peak positions show a systematic displacement with temperature. A temperature-difference analysis shows that the peak intensities do not change and consequently there appears to be no growth of this phase into the entrance volume of the pores. A close examination of the peak profiles for ice reveals a systematic displacement in the Q-value as the temperature is increased, corresponding to the increase of the lattice constant. Separation of the two crystal contributions is not simple due to the displacement of the peaks from ice I_h with temperature but a preliminary analysis indicates that the main central peak of the composite pattern continues to grow as the temperature falls further. The fourth peak at 2.4 Å^{-1} is due only to the hexagonal phase and does not change in intensity. The fifth peak at

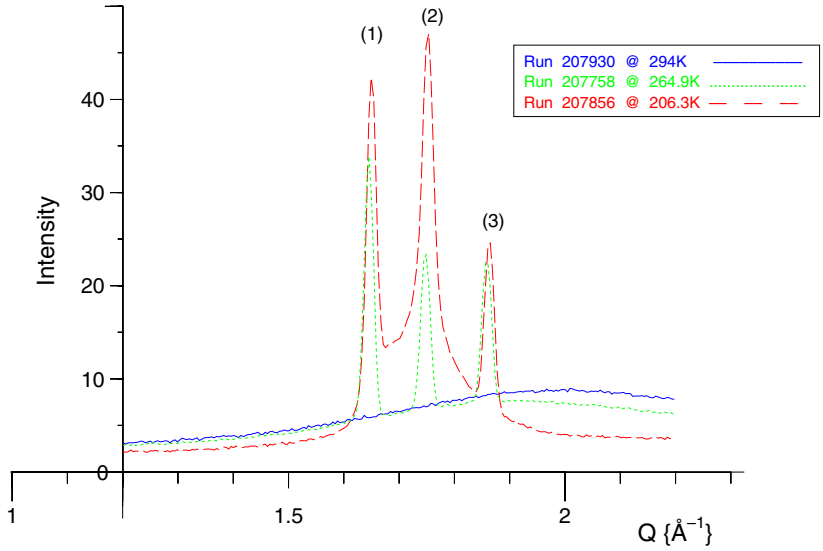

Figure 5. The variation of the profile for the main diffraction peaks for water in SBA-15 (sample A1) at different temperatures; see the text for details.

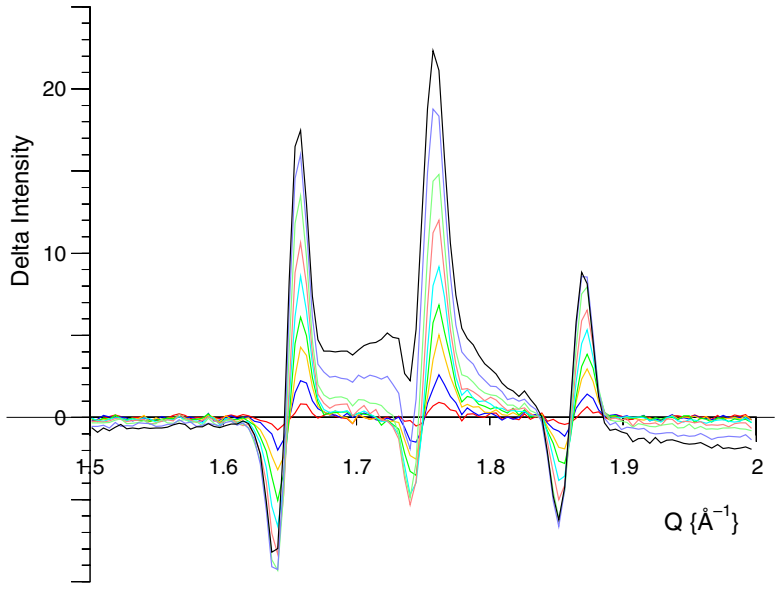

Figure 6. The temperature difference function for water/ice in SBA-15 (sample A1), showing the displacement of the hexagonal ice peaks and the growth of cubic ice, 188–270 K.

2.8 Å^{-1} comprises a sharp peak from the hexagonal ice and a broad peak from the cubic ice. Further information may also be obtained from the eight peaks at higher Q-values, and data analysis is proceeding.

Figure 6 shows $\Delta D_{\mathrm{M}}(Q, T; T_0)$ across an 82 °C range, indicating the differential form arising from the displacement of the sharp peak from ice $\mathrm{I_h}$ and the continuing growth of the central peak of the triplet. Although a full quantitative treatment is not complete and will be

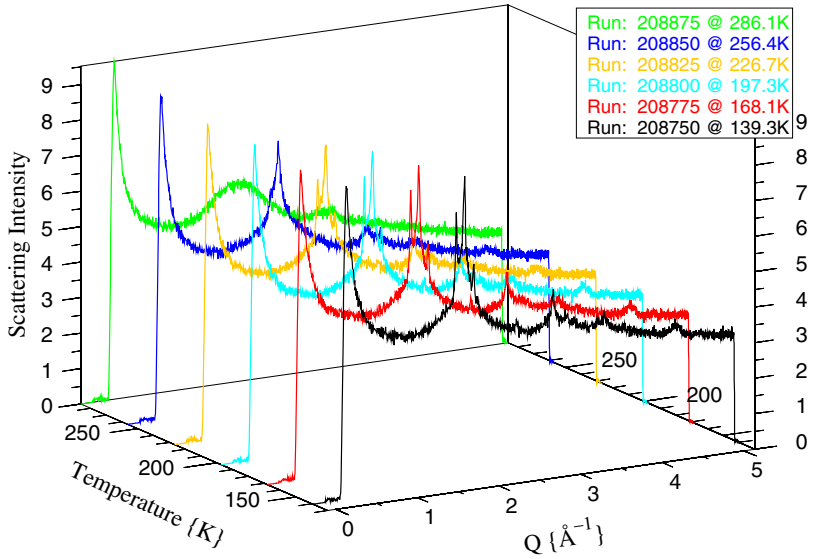

Figure 7. The diffraction pattern for water/ice in an under-filled sample of SBA-15 silica (sample A2) as a function of temperature during a warming ramp.

reported separately, it seems clear that there is a conversion of a supercooled liquid or glassy form of ice into a crystalline form in the lower temperature range of the cooling run. Since the pores are completely filled with water under ambient conditions, it seems likely that this crystal growth comes from the conversion of a disordered water phase at the water–silica interface into cubic ice. The nucleation process is therefore not a unique event but is spread over a range of temperatures. Furthermore, it seems that the diffraction profile of the defective cubic ice formed in these silicas is very similar to that seen in both the MCM and sol–gel silicas.

The main phase transitions in SBA-15 show features similar to those seen in DSC and NMR cryoporometry studies of sol–gel silicas (Strange *et al* 2003, Dore *et al* 2004); however, neutron diffraction in addition provides data on the crystalline form of the ice. The melting point of the cubic ice in the pores is depressed below the bulk T_m by just ΔT_{GT}, while the hexagonal ice around the grains melts at T_m. Nucleation is a statistical process that leads to a greater variability in T_{sc} than in T_m, particularly under conditions of partial filling where different regions of the metastable liquid may nucleate at different temperatures. These studies indicate that, as well as the bulk liquid supercooling below T_m by ΔT_{scB}, the liquid in the pores supercools below $T_m - \Delta T_{GT}$ by an additional ΔT_{scP}.

The diffraction results for the under-filled sample A2 are shown in figure 7 for a warming cycle, following a cooling sequence down to 140 K. There is a difference between the freezing and melting temperatures in this case and it is therefore convenient to show the melting point behaviour. In this case the pores are not completely filled and the behaviour is modified, as observed by Findenegg (Schreiber *et al* 2001). The sequence of measurements for a cooling run reveals the initial formation of the cubic ice in the pores as expected. However, at lower temperatures there is a surprising emergence of the hexagonal ice features and a growth of the definitive peak at 2.4 Å^{-1} that is only present in the ice I_h pattern. The variation of the triplet peak profile during the warming ramp is shown in figure 8.

Previous studies on sol–gel silicas (Dore 2000) had led to the belief that hexagonal ice would not be formed in pores of less than 300 Å in diameter. It now seems that there is

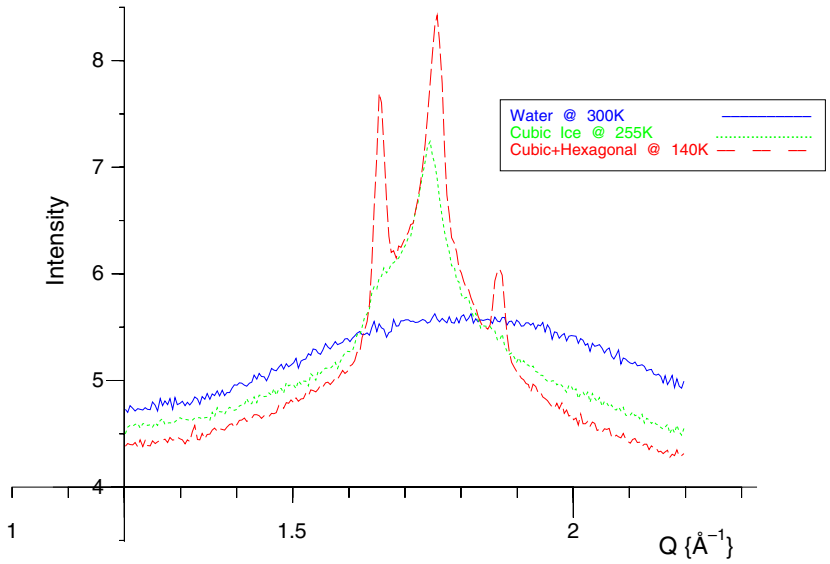

Figure 8. The variation of the peak profile for water in under-filled SBA-15 (sample A2) as a function of temperature during a warming ramp.

initial nucleation of cubic ice in the pores but a growth mechanism leading to the formation of hexagonal ice starts at a slightly lower temperature. A detailed quantitative treatment of the structural changes for this interesting behaviour has yet to be conducted but it seems to suggest that the unusual results obtained in the DSC studies relate to a complex nucleation and growth process that is influenced by the filling factor. If disordered water or a glassy form of ice is present at the silica walls as a connected layer, it is possible that this phase may nucleate in a different manner and that the hexagonal ice crystallites can grow along the cylinder axis of the pores. The high Q-resolution of the present measurements should enable the diffraction broadening features to be extracted and the overall crystal dimensions to be evaluated. These results therefore provide information on the complex water–ice transformation process, but a detailed analysis procedure will be required to extract further quantitative information.

A recent x-ray study of partially filled SBA-15 with a mean pore diameter of 78 Å has been made (Morishige and Iwasaki 2003), over a restricted Q-range using laboratory equipment. A surprising observation is that the solid phase does not exhibit the triplet peaks at $\approx$1.7 Å seen in the present neutron data, although this may be due to instrumentation limitations. There is however a clear indication of the nucleation event. This lack of sharp ice peaks may possibly be due to the smaller pore size but could also indicate an increase in the defective component or smaller crystallite size, leading to a broadening of the peaks. The other feature emerging from the study is the sensitivity of the nucleation process to the filling factor, f, which is attributed to variation of the water film or droplet concentration. The conclusions are broadly in agreement with other work on SBA-15 (Schreiber *et al* 2001) and the observations of the partially filled study (sample A2) given here.

4.3. NMR studies

Various studies have been performed on water and ice in MCM41 and MCM48 silicas (Hansen *et al* 1997). The small pore diameters result in nearly all the water being within several

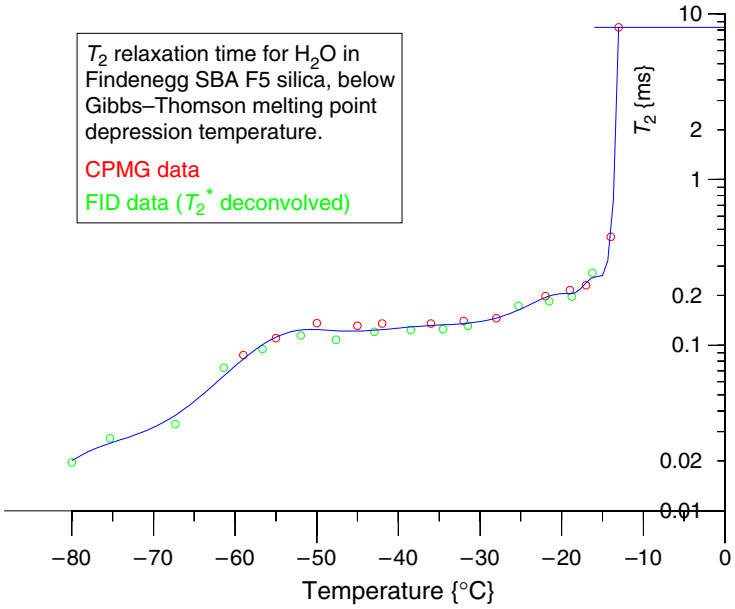

Figure 9. The variation in the NMR proton T_2 relaxation time as a function of temperature for water in SBA-15 (sample A), overfilled.

molecular diameters of a silica interface. This situation results in a fast T_2 relaxation in the water and a longer than usual T_2 relaxation time for any ice that is formed in the pores. Temperatures of $<$200 K are required to completely freeze water in these pores and some thermal studies based on differential scanning calorimetry (DSC) appear to indicate that freezing is not observed. When nucleation is observed in NMR studies, the ice formed is sufficiently mobile that the T_2 relaxation time is far longer than bulk ice, approaching that of the liquid in the pores. These systems will need further investigation to understand the behaviour of the water/ice in the pores but this study is hampered by the narrow range of pore diameters, typically 25–35 Å, that are available for MCM samples, making it difficult to distinguish between bulk and interfacial properties.

The SBA silicas are available with a wider range of larger pore diameters than the MCM silicas. Importantly, the distribution of pore diameters in an SBA sample is narrower than in sol–gel silicas, implying a sharper transition for the Gibbs–Thomson depressed melting point $T_m(x)$. One disadvantage in the use of SBA silicas is the current uncertainty associated with the fundamental definition of the actual pore characteristics. Several groups (Joo *et al* 2002) have claimed that there is a microporous component that links the cylindrical channels or alternatively that the walls of the channels are significantly deformed from a smooth interface.

Figure 9 shows preliminary relaxation results obtained for a highly overfilled SBA-15 silica sample, from the same batch as sample A used for the neutron measurements. The curve, $T_2(T)$, shows changes in the NMR proton transverse relaxation time as the water in SBA silica is warmed from a deeply frozen state. This graph reveals useful information about the dynamics of the water/ice in the sample and its proximity to the silica interface. The T_2 relaxation time is a measure of the strength of the interaction between the neighbouring proton nuclear spins. In particular, a long T_2 relaxation time is indicative of the presence of motion, which serves to average the dipolar interactions that cause T_2 relaxation.

At the highest temperatures, the sample has a constant T_2 relaxation time of about 8 ms, which indicates there is liquid water in the pores. The T_2 relaxation time for pure water is of the order of a few seconds and this faster relaxation time is mainly due to the exchange of magnetization at the pore–water interface. The ice formed in the pores of sample A melts with a value of $\Delta T_{GT} = 14.0\,^{\circ}\mathrm{C}$ in this experiment. This value is very comparable with the $\Delta T_{GT} = 14.0\,^{\circ}\mathrm{C}$ observed in the earlier neutron diffraction measurements. More precise NMR cryoporometry results with a slower temperature ramp, using a similar analysis to that used in the neutron scattering case, indicate that ΔT_{GT} may actually be nearer to 13.5 °C. Using equation (9) to deduce pore dimensions with $k_{GT} = 582$ K Å as derived for sol–gel silicas (Webber 2000, Webber *et al* 2001), gives a pore diameter of 43 Å, significantly different from the nominal dimensions of 92 Å as obtained from a BJH analysis of N_2 condensation data (Findenegg, private communication). However, the Gibbs–Thomson equation is the constant pressure analogue of the constant temperature Kelvin equation for the case of evaporation from the pores; inserting the N_2 evaporation pressure into the Kelvin equation gives a diameter of about 56 Å. Since the geometry of these pores is known to be cylindrical, whereas the sol–gel geometry for which this k_{GT} was obtained may on average be described as intersecting spherical voids, it may be possible to combine dimensional measurements from other techniques, such as SANS, to obtain experimental data on the effect of geometry in the Gibbs–Thomson relationship (Webber 2000, Webber *et al* 2001).

The T_2 relaxation time for bulk ice is of the order of 10 μs or less. The measured relaxation has a Gaussian component, as expected, that corresponds to both the bulk brittle ice around the grains, and some brittle ice in the pores. Figure 9 indicates that, over a temperature range of −55 to −12 °C, the ice in the SBA pores also displays a component with a longer T_2 relaxation time in the region of 100–200 μs. Therefore it is possible to conclude that this form of 'water/ice' displays a significant proton mobility that is intermediate between that of bulk ice and bulk water. This result is presumably related to the features of the neutron diffraction patterns for this temperature region, where a significant disordered component is seen, and in addition the peaks show the dominant structure of defective cubic ice. At lower temperatures the T_2 of the more mobile component is reduced, the relaxation curve becomes more Gaussian-like and its amplitude reduces, while the amplitude of the signal from the brittle ice component increases. This behaviour indicates the conversion of mobile ice to brittle ice at lower temperatures, corresponding to the neutron case of conversion of the disordered component to an ordered ice. The plateau in the relaxation rate has a lower transition temperature, which occurs over the temperature range of −68 to −54 °C. It is not clear at this stage whether this behaviour may be interpreted using the Gibbs–Thomson relationship to deduce the presence of a surface film or other region of increased proton mobility, with dimensions of the order of 9 Å. If so, this may imply a local change to the Gibbs free energy, due to the surface interaction energy terms. It is also possible that this feature could relate to the microporous channels that have been reported in SBA-15 as bridging across the main cylindrical pores (Joo *et al* 2002), although they are not seen in DCS measurements on these actual samples (Schreiber *et al* 2001). Below −55 °C, the mobility of the ice in the SBA pores reduces towards that of bulk ice but it is still not as rigid as that of the normal ice phase even at −80 °C. At this stage of the interpretation, further NMR work needs to be performed to distinguish between the properties of the body of the defective ice in the pores and that of any interfacial layer that may be more mobile. Partial-filling studies should aid this understanding.

The observed changes in the relaxation time from their bulk values, for both the water and ice, imply that NMR cryoporometry must be applied with care to interpret the dynamical properties of the system being studied. Initially, cryoporometry was performed using a single constant measurement time (that of the spin echo) but it now seems preferable, in these more

complex systems, to measure the full relaxation curve and only then to interpret this information to distinguish and separate the water and ice components (Strange *et al* 2003). With these precautions, SBA silicas form a promising material with which to study the dynamics and structure of water/ice systems in confined geometry, in general, and the properties of the water/ice to silica interfaces, in particular. However, a better understanding of the liquid–substrate interaction will only be achieved by a wider investigation involving various liquids in a range of mesoporous materials.

4.4. Interpretation

The present results have indicated that the creation of ice in a constricted volume involves a complex process of nucleation and growth in which temperature, time and geometry play a decisive role. The behaviour of the water and ice in the completely filled pores is the most easily interpreted, as the confined water volume is fully connected within each individual cylinder and the ice crystallites can therefore grow along the axis. In the small-diameter pores of the MCM silicas, there is deep supercooling of the water prior to nucleation and it is believed that nucleation occurs at various points along the cylinder axis. Sufficient nucleation sites are created such that the subsequent growth of the cubic ice phase leads to a large number of individual crystallites. This situation seems to be repeated in the filled SBA silicas and the diffraction pattern indicates that a similar kind of disorder occurs in the alignment of the growth planes.

It is assumed that the nucleation event occurs in the main volume of the liquid and not at the interface with the silica walls. Various computer studies have suggested that the hydrophilic surface causes a specific structural arrangement of the water layer at the interface which behaves differently from the rest of the liquid. Earlier experimental studies suggested that this 'contact' region could be regarded as an 'unfreezable' water layer. The present experimental results seem to indicate that this layer which is restricted to a few monolayers has a complex behaviour as a function of temperature in terms of both structure and dynamics.

The neutron scattering results in SBA silica demonstrate that below the Gibbs–Thomson melting point some of the water/ice in the pores is defective cubic ice but there is also a contribution that resembles the disordered characteristics typical of water. The latter feature diminishes in amplitude at lower temperatures but still persists below $-50\,^{\circ}$C. A corresponding situation exists in the case of the NMR relaxation results where the signal is partially that from brittle ice and partially that from a more mobile component that persists below $-50\,^{\circ}$C, that also reduces in amplitude at lower temperatures. Some NMR experiments would fail to distinguish this mobility from that of water. These results indicate that the phase is an order of magnitude more mobile than brittle ice (NMR) and is disordered (NS). However, the NMR data show that this component is much closer in its mobility to ice than water. There is considerable evidence in both the NMR and scattering literature to suggest that these observations are due to a mobile disordered layer at the silica surface. It now seems that the effective thickness and mobility of the disordered 'quasi-liquid' layer changes gradually with reducing temperature after the main nucleation event has occurred but confirmation of this interpretation will require further work. It is also possible that the very recent x-ray reflectivity measurements (Engemanni *et al* 2004) for a bulk ice–silica surface may be explained in similar terms, relating to the changes in the 'quasi-liquid-like' layer with temperature.

The results for the partially filled SBA-15 silicas are complex and seem to indicate a separation of the nucleation and growth processes. In this case, the initial formation of cubic ice seems to be followed by a separate phase in which hexagonal ice grows along the cylinder axis and there is a conversion of the disordered interfacial layer into the crystalline material as

the temperature is further reduced. The current neutron data also seem to indicate, surprisingly, that this process is reversible on the warming cycle but further analysis will be needed to confirm this finding.

5. Conclusions

The present results have demonstrated that the overall features relating to the supercooled liquid state and the nucleation process are similar in the filled pores of sol–gel and MCM/SBA silicas. However, new features have emerged in the growth of the ice phase due to the different geometry of the pore network.

This type of investigation can now be extended to other situations involving water in confined geometry in which the surface interactions are changed. There is a particular interest in hydrophobic surfaces, which may be achieved by surface modification of the silicas (Dore *et al* 1984, Martin *et al* 2002) or the use of other mesoscopic materials, such as carbon nanotubes (Kaneko *et al*, unpublished results). The further extension into topics related to confined water in bio-systems is also relevant but will probably take a little longer to develop. In conclusion, it seems likely that both neutron diffraction and NMR methods will play a central role in the future experimental techniques.

Acknowledgments

The experimental work conducted at the ILL was supported by the EPSRC of the UK; we wish to thank Thomas Hansen for invaluable assistance during the experiments on D20. The analysis for sample A was conducted by Eric Liu as a part of his MSc Thesis project. The NMR cryoporometry experiments were conducted at the University of Kent using facilities originally developed as part of a PhD Thesis (Webber 2000).

References

Allen S G, Mallett M J D and Strange J H 2001 *J. Chem. Phys.* **114** 3258–64
Allen S G, Stephenson P C L and Strange J H 1998 *J. Chem. Phys.* **108** 8195–8
Alnaimi S M, Mitchell J, Strange J H and Webber J B W 2004 *J. Chem. Phys.* **120** 2075–7
Alnaimi S M, Strange J H and Smith E G 1994 *Magn. Reson. Imaging* **12** 257–9
Bahceli S, Al-Kaisi A R S, Krynicki K and Strange J H 1991 *Characterisation of Porous Solids II* (*Studies in Surface Science and Catalysis* vol 62) ed F Rodriguez-Reinoso, J Rouquerol, K S W Sing and K K Unger (Amsterdam: Elsevier) pp 293–300
Baker J M, Dore J C and Behrens P 1997 *J. Phys. Chem.* B **101** 6226–9
Booth H F and Strange J H 1998a *Magn. Reson. Imaging* **16** 501–4
Booth H F and Strange J H 1998b *Mol. Phys.* **93** 263–9
Brownstein K R and Tarr C E 1977 *J. Magn. Reson.* **26** 17–24
Brun M, Lallemand A, Quinson J-F and Eyraud C 1977 *Thermochim. Acta* **21** 59–88
Bruni F, Ricci M A and Soper A K 1998 *J. Chem. Phys.* **109** 1478–85
Callaghan P T, Godefroy S and Ryland B N 2003 *J. Magn. Reson.* **162** 320–7
Christenson H K 2001 *J. Phys.: Condens. Matter* **13** R95–133
Codd S L and Callaghan P T 1999 *J. Magn. Reson.* **137** 358–72
Coelingh M B 1938 *PhD Utrecht*
Cohan L H 1938 *J. Am. Chem. Soc.* **60** 433
Crupi V, Majolino D, Migliardo P, Venuti V and Bellissent-Funel M C 2003 *Mol. Phys.* **101** 3323–33
Defay R, Prigogine I, Bellemans A and Everett D H 1951, 1966 *Surface Tension and Adsorption* English edn (London: Longmans Green)
Dore J 2000 *Chem. Phys.* **258** 327–47

Dore J, Webber B, Behrens P, Haggenmuller C and Montague D 2002a *New Kinds of Phase Transitions: Transformation in Disordered Substances* (*Nato Science Series, Series II: Mathematics, Physics And Chemistry*) 81st edn, ed V V Brazhkin, S V Buldrev, V N Ryzhov and H E Stanley (Dordrecht: Kluwer–Academic) pp 469–80
Dore J, Webber B, Hartl M, Behrens P and Hansen T 2002b *Physica* A **314** 501–7
Dore J C 1985 *Water Science Reviews* vol 1, ed F Franks (Cambridge: Cambridge University Press) p 45
Dore J C 1991 *Molecular Liquids: New Perspectives in Physics and Chemistry* ed J J C Teixeira-Dias (Dordrecht: Kluwer) p 45
Dore J C, Behrens P and Fisher H 1999 *ILL Annual Report* 28
Dore J C and Blakey D M 1995 *J. Mol. Liq.* **65** 85–90
Dore J C, Coveney F and Bellissent-Funel M-C 1984 *Recent Developments in the Physics of Fluids* ed W S Howells and A K Soper (London: Institute of Physics Publishing) chapter 4
Dore J C and North A N 1991 *Characterisation of Porous Solids II* (*Studies in Surface Science and Catalysis* vol 62) ed F Rodriguez-Reinoso, J Rouquerol, K S W Sing and K K Unger (Amsterdam: Elsevier) pp 245–55
Dore J C, North A N and Rigden J S 1995 *Radiat. Phys. Chem.* **45** 413–26
Dore J C, Sufi M A M and Bellissent-Funel M C 2000 *Phys. Chem. Chem. Phys.* **2** 1599–602
Dore J C, Webber J B W and Strange J H 2004 *Colloids Surf.* A **241** 191–200
Engemanni S, Reicherti H, Doschi H, Bilgrami J, Honkimakii V and Snigirevi A 2004 *Phys. Rev. Lett.* **92** 205701
Eyraus C, Quinson J F and Brun M 1988 *Characterisation of Porous Solids* (Amsterdam: Elsevier)
Farman H, Dore J C and Webber J B W 2002 *J. Mol. Liq.* **96/97** 353–62
Findenegg G H 2003 private communication
Geier O, Snurr Randall Q, Stallmach F and Kärger J 2004 *J. Chem. Phys.* **120** 367–73
Gelb L, Gubbins K E, Radhakrishnan R and Sliwinska-Bartkowiak M 1999 *Rep. Prog. Phys.* **62** 1573–659
Gibbs J W 1906 *Thermodynamics* (*The Scientific Papers of J Willward Gibbs* vol 1) New Dover edn (New York: Dover) (London: Constable) (reprinted 1961)
Gibbs J W 1928 *Collected Works* (New York: Longmans Green)
Gibson I P and Dore J C 1983 *Mol. Phys.* **48** 1019–30
Gore J C, Anderson A W, Does M D, Gochberg D F, Joers J M, Kennan R P, Parsons E C and Schachter M 2001 *Magn. Reson. Imaging* **19** 295–300
Gregg S J and Sing K S W 1967 *Adsorption, Surface Area and Porosity* 2nd edn (London: Academic)
Halperin W P, Bhattacharja S and d'Orazio F 1991 *Magn. Reson. Imaging* **9** 733–7
Hansen E W, Schmidt R and Stocker M 1997 *Stud. Surf. Sci. Catal.* A–C **105** 543–50
Hansen E W, Stocker M and Schmidt R 1996 *J. Phys. Chem. US* **100** 2195–200
Hansen E W *et al* 2002 *J. Phys. Chem.* B **106** 12396–406
Hansen T 2004 *The D20 Instrument Description* http://whisky.ill.fr/YellowBook/D20/
Jackson C L and McKenna G B 1990 *J. Chem. Phys.* **93** 9002–11
Jallut C, Lenoir J, Bardot C and Eyraud C 1992 *J. Membr. Sci.* **68** 271–82
Joo S H, Ryoo R, Kruk M and Jaroniec M 2002 *J. Phys. Chem.* B **106** 4640–6
Kaneko K, Tanaka H, Ohta T, Dore J C, Burian A and Hannon A C 2004 unpublished results
Kimmich R 2002 *Chem. Phys.* **284** 253–85
Levitz P, Korb J-P and Petit D 2003 *Eur. Phys. J.* E **12** 29–33
Martin T, Lefevre B, Brunel D, Galarnea A, Renz F Di, Fajul F, Gobi P F, Quinson J F and Vigier G 2002 *Chem. Commun.* **1** 24–5
McDonald P and Strange J 1998 *Phys. World* **11** 29–34
Mitzithras A, Coveney F M and Strange J H 1992 *J. Mol. Liq.* **54** 273–81
Morineau D and Alba-Simionesco C 2003 *J. Chem. Phys.* **118** 9389–400
Morishige K and Iwasaki H 2003 *Langmuir* **19** 2808–11
Overloop K and van Gerven L 1993 *J. Magn. Reson.* **101** 179–87
Paoli H, Methivier A, Jobic H, Krause C, Pfeifer H, Stallmach F and Kärger J 2002 *Micropor. Mesopor. Mater.* **55** 147–58
Schreiber A, Ketelsen I and Findenegg G H 2001 *Phys. Chem. Chem. Phys.* **3** 1185–95
Sliwinska-Bartkowiak M, Gras J, Sikorski R, Radhakrishnan R, Gelb L and Gubbins K E 1999 *Langmuir* **15** 6060–9
Soper A K 1994 *J. Chem. Phys.* **101** 6888–901
Soper A K, Bruni F and Ricci M A 1998 *J. Chem. Phys.* **109** (4)
Stallmach F and Kärger J 1999 *J. Int. Adsorpt. Soc.* **5** 117–33
Stapf S, Kimmich R and Seitter R-O 1996 *Magn. Reson. Imaging* **14** 841–6
Steytler D C, Dore J C and Wright C J 1983 *Mol. Phys.* **48** 1031–51
Strange J H 1994 *Nondestruct. Test. Eval.* **11** 261–71
Strange J H, Mitchell J and Webber J B W 2003 *Magn. Reson. Imaging* **21** 221–6

Strange J H, Rahman M and Smith E G 1993 *Phys. Rev. Lett.* **71** 3589–91
Strange J H and Webber J B W 1997a *Appl. Magn. Reson.* **12** 231–45
Strange J H and Webber J B W 1997b *Meas. Sci. Technol.* **8** 555–61
Strange J H, Webber J B W and Schmidt S D 1996a *Magn. Reson. Imaging* **14** 803–5
Strange J H *et al* 1996b *Magn. Reson. Imaging* **14** 963–5
Sufi M A M 1984 Neutron diffraction studies of super-cooled liquid heavy water *MSc Physics* University of Kent at Canterbury, UK
Tell J L and Maris H J 1983 *Phys. Rev.* B **28** 5122–5
Thomson J 1849 *Trans. R. Soc. Edinburgh* **16** 575–80
Thomson J 1862 *Proc. R. Soc.* **11** 473–81
Thomson J J 1888 *Application of Dynamics to Physics and Chemistry* (London: Macmillan)
Thomson W 1871 *Phil. Mag.* **42** 448–52
Valiullin R, Furó I, Skirda V and Kortunov P 2003 *Magn. Reson. Imaging* **21** 299–303
Webber J B W 2000 The characterisation of porous media *PhD Physics* University of Kent at Canterbury, UK http://www.kent.ac.uk/physical-sciences/publications/theses/jbww.html
Webber J B W, Strange J H and Dore J C 2001 *Magn. Reson. Imaging* **19** 395–9
Young T 1805 *Phil. Trans. R. Soc.* **95** 65
Young T 1855 *Miscellaneous Works of the Late Thomas Young* vol 1, ed G Peacock (Albemarle Street, London: John Murray) chapter XIX, pp 418–53